Phase-matching condition in rotatory nonlinear optics

Chen Cui, Fei Liang, Dazhi Lu, Haohai Yu [ORCID],[*] and Huaijin Zhang[†]

State Key Laboratory of Crystal Materials and Institute of Crystal Materials, Shandong University, Jinan 250100, China

Polarization rotation of light beams, such as optical activity and Faraday rotation, is a natural effect that generates the rotation of the polarized direction of light and some undiscovered characteristics in nonlinear optics. In our previous study, we theoretically investigated the second-harmonic generation process in rotatory nonlinear optics and found an unprecedented phase-matching condition. Here, the optical phase-matching condition in the second-harmonic generation with rotatory polarization is theoretically analyzed and associated with the angular rotation-induced phases of mixing waves, which goes beyond the previous theoretical analysis. Moreover, the Pancharatnam-Berry topological phase was found to be periodically generated and could be employed to compensate for the mismatched phase during nonlinear optical interaction. Possible experimental schemes were proposed and discussed. This work provides not only a universal and flexible (quasi-) phase-matching condition for the rotatory nonlinear optics existing in most nonlinear optical media but may also inspire the development of modern photonics.

I. INTRODUCTION

Nonlinear frequency conversion has been applied to classical and quantum optics since the discovery of nonlinear second-harmonic generation (SHG) in 1961 [1], which subsequently boosted the discovery of many nonlinear optical effects [2–6]. The phase-matching (PM) condition, which describes the momentum relationship among the interacting light, is the most critical factor when ensuring highly efficient nonlinear frequency conversion. In 1962, birefringent PM and quasi-phase-matching (QPM) conditions were theoretically proposed [7], which laid the theoretical foundations for nonlinear optics. To date, most descriptions of PM conditions in nonlinear optics are based on linearly polarized light corresponding to the general birefringence, where two orthonormalized linear polarization states can be used as a set of basis vectors to describe the possible linear polarization states. However, in addition to linear polarization, circular birefringence (or circular dichroism) also exists in nature and presents itself as the rotation of linear polarization in realistic materials with helical structures [8]. From the viewpoint of crystallography, SHG can be generated in acentric crystals belonging to 20 different types of point groups, and among them, materials belonging to a possible 15 types of point groups could perform circular dichroism characterization, which means that the rotation performance of the polarization exhibited in nonlinear optics would be significant in the development of the theory of nonlinear optics and future photonics. In fact, little attention has been paid to the role of polarization rotation [9,10] because current nonlinear optical materials that are based on linear polarization have negligible optical activity, which limits the development and discovery of rotatory nonlinear optics.

In rotation linear optics, the Pancharatnam-Berry (PB) topological phase is an important signature and was first demonstrated by Pancharatnam while investigating the phase relationship during the evolution of polarization states [11]. In 1986, experimental verification of the PB topological phase was observed in an optical fiber [12]. In 1987, Berry [13] unified and extended the theory of the geometric phase, which inspired the recent theoretical and experimental development of the higher-order PB phase [14]. Given the established PM conditions, the PB topological phases should undoubtedly contribute to the nonlinear optical process, but these have not yet been explored. Herein, we theoretically study the SHG with rotatory polarization and achieve the QPM conditions in rotatory nonlinear optics based on the analysis of the angular velocity. In addition, we also find that the PB topological phases could be periodically generated and employed to compensate for the mismatched phase, and hence the realization of a QPM technique in rotatory nonlinear optics is made possible.

II. EFFECTIVE ELECTRIC POLARIZATION AND EFFECTIVE NONLINEAR COEFFICIENT

The SHG process in optically rotatory and nonlinear crystals is shown in Fig. 1(a). A fundamental beam enters the crystal at normal incidence, and the driving electric polarization vector of the SHG is generated. The fundamental wave in the crystal is $\vec{E}^{\omega}(r)$. The incident direction of the initial fundamental wave can be expressed as $\hat{v} = \begin{pmatrix} \sin\theta\cos\psi \\ \sin\theta\sin\psi \\ \cos\theta \end{pmatrix}$, where θ is the angle between the z axis and $\hat{v}$, ψ is the angle between the x axis and the projection of $\hat{v}$ in the xy plane, and $\hat{v}$ is a unit vector. The initial fundamental wave is assumed to be perpendicular to the z axis and can be expressed as $\vec{E}^{\omega}(0) = |\vec{E}^{\omega}(0)| \begin{pmatrix} \sin\psi \\ -\cos\psi \\ 0 \end{pmatrix}$ to simplify the solution, which does not impact the PM or QPM results. In the rotatory crystal, the

[*]haohaiyu@sdu.edu.cn
[†]huaijinzhang@sdu.edu.cn

fundamental electric field rotates dynamically, which means that the direction of the induced electric polarization vector gradually changes. As shown in Figs. 1(a) and 1(b), when the fundamental wave propagates from the position 0 to r, the rotation angle of the polarization state is $\rho_1 r$, where ρ_1 is

$$
\boldsymbol{R}(\alpha) = \begin{pmatrix} \cos\alpha + r_1^2(1-\cos\alpha) & r_1 r_2(1-\cos\alpha) - r_3\sin\alpha & r_1 r_3(1-\cos\alpha) + r_2\sin\alpha \\ r_2 r_1(1-\cos\alpha) + r_3\sin\alpha & \cos\alpha + r_2^2(1-\cos\alpha) & r_2 r_3(1-\cos\alpha_1) - r_1\sin\alpha \\ r_3 r_1(1-\cos\alpha) - r_2\sin\alpha & r_3 r_2(1-\cos\alpha) + r_1\sin\alpha & \cos\alpha_1 + r_3^2(1-\cos\alpha) \end{pmatrix}, \tag{1}
$$

where r_1, r_2, and r_3 are the magnitudes of the wave components along the x-, y-, and z axes, respectively. Therefore, the electric field of the fundamental wave at position r is expressed as

$$
\vec{E}^\omega(r) = |\vec{E}^\omega(r)| \begin{pmatrix} \sin\rho_1 r \cos\theta \cos\psi + \cos\rho_1 r \sin\psi \\ \sin\rho_1 r \cos\theta \sin\psi - \cos\rho_1 r \cos\psi \\ -\sin\rho_1 r \sin\theta \end{pmatrix}. \tag{2}
$$

The dynamic electric polarization vector generated by the interaction of the rotating fundamental wave and the nonlinear crystal can be expressed as a function of r, such that $\vec{P}^{2\omega}(r) = \varepsilon_0 \boldsymbol{d} : \vec{E}^\omega(r)\vec{E}^\omega(r)$, where ε_0 is the permittivity of free space, and $\boldsymbol{d}$ is the matrix of second-order nonlinear coefficients. In addition, the component of $\vec{P}^{2\omega}(r)$ parallel to $\vec{r}$ should be neglected because the second-harmonic (SH) electric field can only be generated in the direction perpendicular to $\vec{v}$. Hence, the contributing part is the component perpendicular to $\vec{P}^{2\omega}(r)$, which is given by $\vec{P}_\perp^{2\omega}(r) = \vec{P}^{2\omega}(r) - \vec{P}_\parallel^{2\omega}(r)$ as schematically shown in Fig. 1(b). The differential unit of the incremental SH wave, dr, at position r can be written in a differential form as $d\vec{E}^{2\omega,r}$, which is proportional and parallel to $\vec{P}_\perp^{2\omega}(r)$ and expressed as $d\vec{E}^{2\omega,r} \propto \vec{P}_\perp^{2\omega}(r) \cdot dr$. As shown in Fig. 1(c), when the incremental SH wave generated at r travels from r to the exit face L, the vector $d\vec{E}^{2\omega,r}$ rotates at an angle of $\rho_2(L-r)$ and can be rewritten as $\boldsymbol{R}_2 d\vec{E}^{2\omega,r}$, where $\boldsymbol{R}_2 = \boldsymbol{R}(\rho_2(L-r))$ is the matrix for the rotation angle $\rho_2(L-r)$ around the axis of $\vec{v}$, and ρ_2 is the rotational angular velocity of the SH polarization plane. Therefore, $\boldsymbol{R}_2 \vec{P}_\perp^{2\omega}(r)$ can be considered as an effective electric polarization vector and can be written as $\vec{P}_{\text{eff}}^{2\omega}(r) = \boldsymbol{R}_2 \vec{P}_\perp^{2\omega}(r)$. The effective nonlinear coefficient for the rotation SHG, $\vec{d}_{\text{eff}}(r)$, can then be obtained from the expression $\vec{P}_{\text{eff}}^{2\omega}(r) = \varepsilon_0 \vec{d}_{\text{eff}}(r)|\vec{E}^\omega(r)||\vec{E}^\omega(r)|$.

III. PHASE-MATCHING CONDITION OF ROTATORY ELECTRIC FIELDS

Here, we express the fundamental wave, $\vec{E}^\omega$, the output SH wave, $\vec{E}^{2\omega}$, and the effective electric polarization for SHG as:

$$
\vec{E}^\omega = \vec{A}^\omega e^{-i(\omega t - \varphi_{1ol})}, \tag{3}
$$

$$
\vec{E}^{2\omega} = \vec{A}^{2\omega} e^{-i(2\omega t - \varphi_{2ol})}, \tag{4}
$$

$$
\vec{P}_{\text{eff}}^{2\omega}(r) = \boldsymbol{R}_2 \vec{P}_\perp^{2\omega}(r) = \varepsilon_0 \vec{d}_{\text{eff}}(r)|\vec{A}^\omega|^2 e^{-2i(\omega t - \varphi_{1ol})}, \tag{5}
$$

where the vectors $\vec{A}^\omega$ and $\vec{A}^{2\omega}$ represent the complex amplitude in the directions of $\tilde{E}^\omega$ and $\tilde{E}^{2\omega}$, respectively, which

contain no time-variant elements and can be written in the form of Cartesian coordinates, such that $\vec{A}^\omega = \begin{pmatrix} A_1^\omega \\ A_2^\omega \\ A_3^\omega \end{pmatrix}$ and $\vec{A}^{2\omega} = \begin{pmatrix} A_1^{2\omega} \\ A_2^{2\omega} \\ A_3^{2\omega} \end{pmatrix}$; ω is the angular frequency of the fundamental wave; φ_{1ol} and φ_{2ol} are time-independent phases of the fundamental and SH waves, given by $\varphi_{1ol} = k_1 r$ and $\varphi_{2ol} = k_2 r$, respectively, where k_1 and k_2 are the wave number of the fundamental wave and SH wave, respectively. The Maxwell equations describing the SHG in a nonmagnetic material containing no free charges can be expressed as [15]

$$
\nabla^2 \vec{E}^{2\omega} - \mu_0 \varepsilon_0 \varepsilon_{\text{relative}}(\omega) \frac{\partial^2 \vec{E}^{2\omega}}{\partial t^2} = \mu_0 \frac{\partial^2 \vec{P}_{\text{eff}}^{2\omega}}{\partial t^2}, \tag{6}
$$

where μ_0 is the permeability of free space, and $\varepsilon_{\text{relative}}(\omega)$ is the relative permittivity of the material. Substituting Eqs. (3)–(5) in Eq. (6), the following equation can be obtained using the slowly varying amplitude approximation:

$$
\frac{d\vec{A}^{2\omega}}{dr} = \frac{\pi i \vec{d}_{\text{eff}}(r)|\vec{A}^\omega|^2}{n_2 \lambda} e^{i\Delta\varphi_{ol}}, \tag{7}
$$

where n_2 is the refractive index of the material for the SH wave, λ is the SH wavelength, and $\Delta\varphi_{ol}$ is the phase difference caused by the different optical lengths, given by $\Delta\varphi_{ol} = 2\varphi_{1ol} - \varphi_{2ol}$. Supposing that the crystal does not absorb both fundamental and SH waves, and very low optical power is transferred from fundamental to SH wave (small-signal approximation, expressed as $|\vec{A}^\omega(r)| \cong |\vec{A}^\omega(0)|$) [16], the amplitude of fundamental wave $|\vec{A}^\omega|$ is approximately constant.

Without loss of generality, we investigated the rotatory nonlinear optics from the optically rotatory cubic materials belonging to classes 23 and $\bar{4}3m$. Cubic crystals have isotropic refractive indices for any polarization direction and any incident direction, which result in obvious optical rotation [17]. In addition, classes 23 and $\bar{4}3m$ were acentric structures. Therefore, crystals belonging to classes 23 and $\bar{4}3m$ have both obvious optical rotation (and Faraday rotation) and nonlinearity for nearly all incident conditions. With the notation simplified by introducing a contracted matrix d_{il}, the matrix of the second-order nonlinear optical coefficient for cubic nonlinear crystals [18] can be represented as

$$
\boldsymbol{d} = \begin{pmatrix} 0 & 0 & 0 & d_{14} & 0 & 0 \\ 0 & 0 & 0 & 0 & d_{14} & 0 \\ 0 & 0 & 0 & 0 & 0 & d_{14} \end{pmatrix}. \tag{8}
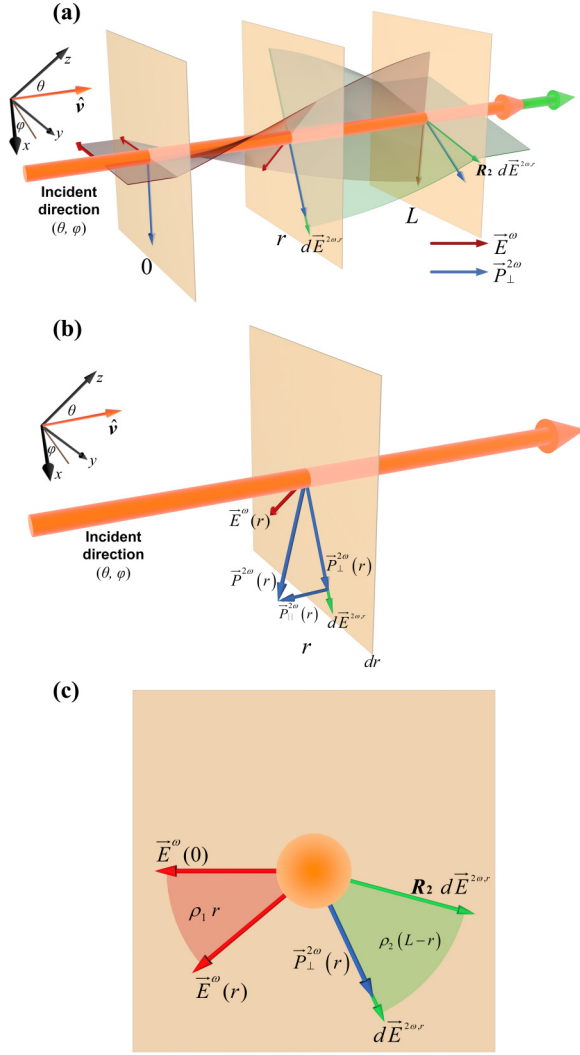$$

FIG. 1. (a) Schematic of how a fundamental beam moves in a rotatory crystal for SHG. (b) Schematic for the electric polarization at the position r in the crystal $\vec{P}^{2\omega}$, $\vec{P}^{2\omega}_\perp$, $\vec{P}^{2\omega}_\parallel$ (blue arrows). (c) Rotation of the fundamental electric field from 0 to r and the incremental SH electric field at r from r to L. The brown planes represent the different positions in the crystal. The plane 0 ($r = 0$) is the incident face. The plane L ($r = L$) is the exit face. The plane r is a certain position between 0 and L, where the fundamental beam travels a distance r from the incident face. The orange (larger) and green (smaller) cylinders with arrowheads indicate the propagations of the fundamental and SH beams, respectively. The twisted shadow regions in red (dark gray) and green (light gray) schematically show the rotations of the fundamental electric field $\vec{E}^\omega$ and the incremental SH wave generated at r. The arrows in red (black) and blue (dark gray) indicate the directions of $\vec{E}^\omega$ and $\vec{P}^{2\omega}_\perp$. The green (light gray) arrows at planes r and L represent $d\vec{E}^{2\omega,r}$ and $\boldsymbol{R}_2 d\vec{E}^{2\omega,r}$. Note that $\vec{E}^\omega$, $\vec{P}^{2\omega}_\perp$, $d\vec{E}^{2\omega,r}$, and $\boldsymbol{R}_2 d\vec{E}^{2\omega,r}$ are all functions of r.

Then, the effective nonlinear coefficient $\vec{d}_{\text{eff}}(r)$ in cubic crystals is shown as Eqs. (A1)–(A4).

By solving Eq. (7) with the boundary condition of $A^{2\omega}_1 = A^{2\omega}_2 = A^{2\omega}_3 = 0$ at $L = 0$, the expression for the components

along the x-, y-, and z axes of $\vec{A}^{2\omega}$ is obtained as follows:

$$
\begin{aligned}
A^{2\omega}_1 = \frac{\pi i |\vec{A}^\omega|^2}{n_2 \lambda} \Bigg[&\frac{e^{i(\Delta k - \rho_2)L} - 1}{\Delta k - \rho_2} X_1 e^{i\rho_2 L} \\
&+ \frac{e^{i(\Delta k + \rho_2)L} - 1}{\Delta k + \rho_2} X_2 e^{-i\rho_2 L} \\
&+ \frac{e^{i(\Delta k - 2\rho_1 + \rho_2)L} - 1}{\Delta k - 2\rho_1 + \rho_2} X_3 e^{-i\rho_2 L} \\
&+ \frac{e^{i(\Delta k + 2\rho_1 - \rho_2)L} - 1}{\Delta k + 2\rho_1 - \rho_2} X_4 e^{i\rho_2 L} \\
&+ \frac{e^{i(\Delta k - 2\rho_1 - \rho_2)L} - 1}{\Delta k - 2\rho_1 - \rho_2} X_5 e^{i\rho_2 L} \\
&+ \frac{e^{i(\Delta k + 2\rho_1 + \rho_2)L} - 1}{\Delta k + 2\rho_1 + \rho_2} X_6 e^{-i\rho_2 L} \Bigg],
\end{aligned}
\tag{9}
$$

$$
\begin{aligned}
A^{2\omega}_2 = \frac{\pi i |\vec{A}^\omega|^2}{n_2 \lambda} \Bigg[&\frac{e^{i(\Delta k - \rho_2)L} - 1}{\Delta k - \rho_2} Y_1 e^{i\rho_2 L} \\
&+ \frac{e^{i(\Delta k + \rho_2)L} - 1}{\Delta k + \rho_2} Y_2 e^{-i\rho_2 L} \\
&+ \frac{e^{i(\Delta k - 2\rho_1 + \rho_2)L} - 1}{\Delta k - 2\rho_1 + \rho_2} Y_3 e^{-i\rho_2 L} \\
&+ \frac{e^{i(\Delta k + 2\rho_1 - \rho_2)L} - 1}{\Delta k + 2\rho_1 - \rho_2} Y_4 e^{i\rho_2 L} \\
&+ \frac{e^{i(\Delta k - 2\rho_1 - \rho_2)L} - 1}{\Delta k - 2\rho_1 - \rho_2} Y_5 e^{i\rho_2 L} \\
&+ \frac{e^{i(\Delta k + 2\rho_1 + \rho_2)L} - 1}{\Delta k + 2\rho_1 + \rho_2} Y_6 e^{-i\rho_2 L} \Bigg],
\end{aligned}
\tag{10}
$$

$$
\begin{aligned}
A^{2\omega}_3 = \frac{\pi i |\vec{A}^\omega|^2}{n_2 \lambda} \Bigg[&\frac{e^{i(\Delta k - \rho_2)L} - 1}{\Delta k - \rho_2} Z_1 e^{i\rho_2 L} \\
&+ \frac{e^{i(\Delta k + \rho_2)L} - 1}{\Delta k + \rho_2} Z_2 e^{-i\rho_2 L} \\
&+ \frac{e^{i(\Delta k - 2\rho_1 + \rho_2)L} - 1}{\Delta k - 2\rho_1 + \rho_2} Z_3 e^{-i\rho_2 L} \\
&+ \frac{e^{i(\Delta k + 2\rho_1 - \rho_2)L} - 1}{\Delta k + 2\rho_1 - \rho_2} Z_4 e^{i\rho_2 L} \\
&+ \frac{e^{i(\Delta k - 2\rho_1 - \rho_2)L} - 1}{\Delta k - 2\rho_1 - \rho_2} Z_5 e^{i\rho_2 L} \\
&+ \frac{e^{i(\Delta k + 2\rho_1 + \rho_2)L} - 1}{\Delta k + 2\rho_1 + \rho_2} Z_6 e^{-i\rho_2 L} \Bigg],
\end{aligned}
\tag{11}
$$

where $\Delta k = 2k_1 - k_2$, X_i, Y_i, and Z_i ($i = 1, 2, 3, 4, 5,$ and 6) are functions of d_{14}, θ, and ψ, but are independent of L, Δk, ρ_1, and ρ_2 [see Eqs. (B1)–(B18)]. These equations indicate that the general PM conditions in rotatory crystals are $\Delta k \pm \rho_2 = 0$, $\Delta k \pm (2\rho_1 - \rho_2) = 0$, and $\Delta k \pm (2\rho_1 + \rho_2) = 0$, which is in line with the previous results from the theoretical analysis of the SHG along the z axis of a crystal of class 32 [9]. The different values of X_i, Y_i, and Z_i indicate that the six PM conditions have different maximum gains. Considering that only one condition can be existent and that

the SH output under the PM condition is much greater than the phase-mismatched output, the other five conditions can be neglected if one condition is realized. According to the relationship between the intensity and the electric field, $I = 2n\varepsilon_0 c A A^*$, where n is the refractive index of the medium, ε_0 is the vacuum permittivity, and c is the speed of light, we can obtain the relative intensity of the output SH radiation:

$$I_i \propto I_1^2 \mathrm{sinc}^2\left(\frac{\Delta k_i L}{2}\right) L^2 (X_i X_i^* + Y_i Y_i^* + Z_i Z_i^*), \quad (12)$$

where I_1 is the intensity of fundamental wave, Δk_i takes the value of $\Delta k - \rho_2$, $\Delta k + \rho_2$, $\Delta k - (2\rho_1 - \rho_2)$, $\Delta k + (2\rho_1 - \rho_2)$, $\Delta k - (2\rho_1 + \rho_2)$, and $\Delta k + (2\rho_1 + \rho_2)$ corresponding to $i = 1$, 2, 3, 4, 5, and 6, respectively. If $\Delta k_i = 0$, the maximum intensity is relatively given by $I_{i\max} \propto I_1^2 L^2 (X_i X_i^* + Y_i Y_i^* + Z_i Z_i^*)$. Therefore, if the fundamental beam and SH beam have the same beam cross section, the maximum conversion efficiency is

$$\eta_{i\max} = \frac{\pi^2 |\vec{A}^\omega|^2}{n_1 n_2 \lambda^2} L^2 (X_i X_i^* + Y_i Y_i^* + Z_i Z_i^*), \quad (13)$$

where n_1 is the refractive index of the material for the fundamental wave.

In certain special cases, the values of X_i, Y_i, and Z_i can be zero. The expressions of the PM condition for class 32 and the corresponding X_i, Y_i, and Z_i are calculated as shown in Appendix C.

For the particular case as shown in Ref. [9] (class 32, $\theta = 0$), it can be obtained that $X_1 = X_2 = X_3 = X_4 = 0$, $Y_1 = Y_2 = Y_3 = Y_4 = 0$, $Z_1 = Z_2 = Z_3 = Z_4 = Z_5 = Z_6 = 0$, $X_5 = \frac{1}{2}i d_{11} e^{-2i\psi}$, $X_6 = \frac{1}{2}i d_{11} e^{2i\psi}$, $Y_5 = \frac{1}{2}d_{11} e^{-2i\psi}$, and $Y_6 = -\frac{1}{2}d_{11} e^{2i\psi}$. Therefore, the PM conditions are simplified as $\Delta k \pm (2\rho_1 + \rho_2) = 0$. In this case, the total intensity of the output SH radiation without neglecting phase-mismatched terms is given by

$$I \propto \frac{1}{2}\{\mathrm{sinc}^2[\Delta k - (2\rho_1 + \rho_2)L/2]$$
$$+ \mathrm{sinc}^2[\Delta k + (2\rho_1 + \rho_2)L/2]\} I_1^2 L^2 d_{11}^2. \quad (14)$$

These results shown above agree well with the results described in Ref. [9].

The above analysis indicates that the presence of the rotational angular velocity ρ provides an additional phase. The angular velocity terms in the equation for the PM conditions, $\Delta\rho$ [$\Delta\rho = \pm\rho_2$, $\pm(2\rho_1 - \rho_2)$, or $\pm(2\rho_1 + \rho_2)$] represent this type of phase difference between the fundamental wave (or rather, electric polarization) and the SH wave. Here we assume that the waves propagate in the z direction; the fundamental and generated SH waves in the crystal with optical rotation can be described by

$$\vec{E}^\omega = A^\omega(\hat{x}\cos\rho_1 z + \hat{y}\sin\rho_1 z)e^{-i(\omega t - k_1 z)}, \quad (15)$$

$$\vec{E}^{2\omega} = A^{2\omega}(\hat{x}\cos\rho_2 z + \hat{y}\sin\rho_2 z)e^{-i(2\omega t - k_2 z)}, \quad (16)$$

where A^ω and $A^{2\omega}$ are the amplitudes, and $\hat{x}$ and $\hat{y}$ are the unit vectors along the x- and y axes, respectively. Equations (15)

and (16) can be written in exponential form as

$$\vec{E}^\omega = \left\{\frac{1}{2}\hat{x}A^\omega e^{-i[\omega t - (k_1 + \rho_1)z]} + \frac{1}{2}\hat{y}A^\omega e^{-i[\omega t - (k_1 + \rho_1)z]}\right\}$$
$$+ \left\{\frac{1}{2}\hat{x}A^\omega e^{-i[\omega t - (k_1 - \rho_1)z]} - \frac{1}{2}\hat{y}A^\omega e^{-i[\omega t - (k_1 - \rho_1)z]}\right\}, \quad (17)$$

$$\vec{E}^{2\omega} = \left\{\frac{1}{2}\hat{x}A^{2\omega} e^{-i[2\omega t - (k_2 + \rho_2)z]} + \frac{1}{2}\hat{y}A^{2\omega} e^{-i[2\omega t - (k_2 + \rho_2)z]}\right\}$$
$$+ \left\{\frac{1}{2}\hat{x}A^{2\omega} e^{-i[2\omega t - (k_2 - \rho_2)z]} - \frac{1}{2}\hat{y}A^{2\omega} e^{-i[2\omega t - (k_2 - \rho_2)z]}\right\}. \quad (18)$$

We found two different phase velocities from Eqs. (17) and (18) according to $\omega/(k_1 + \rho_1)$ and $\omega/(k_1 - \rho_1)$ for $\vec{E}^\omega$, and $2\omega/(k_2 + \rho_2)$ and $2\omega/(k_2 - \rho_2)$ for $\vec{E}^{2\omega}$. The electric polarization $\vec{P}$ can be described as

$$\vec{P} = \vec{P}_1 e^{-i[\omega t - (k_1 + \rho_1)z]} e^{-i[\omega t - (k_1 + \rho_1)z]}$$
$$+ \vec{P}_2 e^{-i[\omega t - (k_1 - \rho_1)z]} e^{-i[\omega t - (k_1 - \rho_1)z]}$$
$$+ \vec{P}_3 e^{-i[\omega t - (k_1 + \rho_1)z]} e^{-i[\omega t - (k_1 - \rho_1)z]}$$
$$= \vec{P}_1 e^{-i[2\omega t - 2(k_1 + \rho_1)z]}$$
$$+ \vec{P}_2 e^{-i[2\omega t - 2(k_1 - \rho_1)z]} + \vec{P}_3 e^{-i(2\omega t - 2k_1 z)}, \quad (19)$$

where $\vec{P}_1$, $\vec{P}_2$, and $\vec{P}_3$ represent the amplitudes in the directions of the three electric polarizations with different phase velocities. Therefore, three different phase velocities in the electric polarizations and two different phase velocities in the SH field can form six pairs of phase velocity matching: $2\omega/2k_1 = 2\omega/(k_2 - \rho_2)$, $2\omega/2k_1 = 2\omega/(k_2 + \rho_2)$, $2\omega/2(k_1 + \rho_1) = 2\omega/(k_2 + \rho_2)$, $2\omega/2(k_1 - \rho_1) = 2\omega/(k_2 - \rho_2)$, $2\omega/2(k_1 + \rho_1) = 2\omega/(k_2 - \rho_2)$, and $2\omega/2(k_1 - \rho_1) = 2\omega/(k_2 + \rho_2)$, corresponding to six PM conditions: $\Delta k \pm \rho_2 = 0$, $\Delta k \pm (2\rho_1 - \rho_2) = 0$, and $\Delta k \pm (2\rho_1 + \rho_2) = 0$, respectively.

IV. QUASI-PHASE-MATCHING EMPLOYING PANCHARATNAM-BERRY PHASES

Considering the PB topological phase generated during the rotatory polarization, the polarization states can be described with the Poincaré sphere, as shown in Fig. 2(a) [19], where the north–south poles and the equator represent the left–right circular polarization and the linear polarization on the Poincaré sphere, respectively. The polarization plane of the linearly polarized states rotates in an optically rotatory crystal, corresponding to the state moving along the equator of the Poincaré sphere. A PB phase would only appear when the polarization state returns to the initial state, which equals half of the solid angle spanning the Poincaré sphere [13]. The generation conditions of the PB topological phase indicate that the propagation of light with left- or right-handed circular polarization cannot give rise to the PB topological phase, and it is only when the polarization plane rotates by 180° in the optically rotatory crystals, corresponding to a point along a closed cycle around the equator on the Poincaré sphere, that the additional phase of π would be generated immediately.

The phase difference between the electric polarization wave and the SH wave is expressed as $\Delta\varphi = 2\varphi_1 - \varphi_2$, and can be resolved by the phase difference caused by the different optical lengths ($\Delta\varphi_{ol}$), rotation angles ($\Delta\varphi_{ro}$), and PB topological phases ($\Delta\varphi_{PB}$). Here, $\Delta\varphi_{ol}$ is defined as $\Delta k r$, $\Delta\varphi_{ro}$ is present in the rotation and eventually expressed as $\Delta\rho r$,
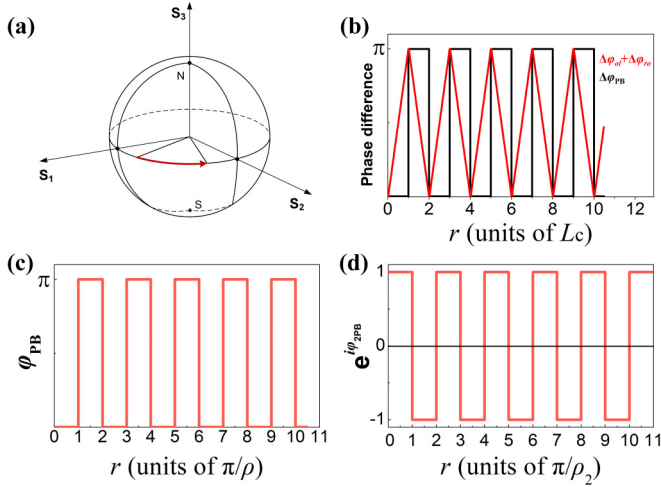
FIG. 2. (a) Illustration of the Poincaré sphere. N/S is the north–south pole; S_1, S_2, S_3 are Stokes parameters. The red line on the equator represents the rotating polarization state in the crystals. (b) Variation of $\Delta\varphi_{ol} + \Delta\varphi_{ro}$ and $\Delta\varphi_{PB}$ as a function of propagation length r. The phases $\Delta\varphi_{ol} + \Delta\varphi_{ro}$ (red) and $\Delta\varphi_{PB}$ (black) change by π when the waves propagate along intervals of the coherence length L_c. In this condition, $\Delta\varphi_{PB}$ can compensate for the phase difference caused by the $\Delta\varphi_{ol}$ and $\Delta\varphi_{ro}$ in SHG. The x axis is in units of L_c, where $L_c = \pi/(\Delta k + \Delta\rho)$. (c) Step function φ_{PB}. PB phase φ_{PB} shift by π when the wave propagates along intervals of distance π/ρ in the optical rotatory crystals. The x axis is in units of π/ρ. (d) Step function $\exp(i\varphi_{2PB})$. The x axis is in units of π/ρ_2.

and $\Delta\varphi_{PB}$ depends on the PB phase of both the fundamental wave φ_{1PB} and the SH wave φ_{2PB}. As shown in Fig. 2(c), φ_{PB} increases by π as the waves propagate. The nonzero sum of $\Delta\varphi_{ol}$ and $\Delta\varphi_{ro}$ in the nonlinear frequency conversion shifts by π when the waves propagate a coherence length of $L_c = \pi/(\Delta k + \Delta\rho)$, and this can periodically modulate the energy conversion from the fundamental wave to the SH wave with a period of π. In SHG, the double PB phase of the fundamental wave is equivalent to zero ($2\varphi_{1PB} = 2\pi$), so that the phase difference from the PB phases is only determined by φ_{2PB}, defined as $\Delta\varphi_{PB} = \varphi_{2PB}$. Therefore, a phase shift of π, arising from the phase difference of the PB phase, appears when the waves propagate a distance of π/ρ_2 in the crystal. If the equation $\pi/\rho_2 = \pi/(\Delta k + \Delta\rho)$ is satisfied, $\Delta\varphi_{PB}$ can periodically compensate for the phase difference caused by $\Delta\varphi_{ol}$ and $\Delta\varphi_{ro}$ in SHG. Thus, the phase condition for QPM, $\Delta\varphi_{PB} = \Delta\varphi_{ol} + \Delta\varphi_{ro}$, is achieved. The changing phase of $\Delta\varphi_{PB}$ and $\Delta\varphi_{ol} + \Delta\varphi_{ro}$ as a function of the propagation length r is shown in Fig. 2(b).

Because the PB topological phase only appears with a phase value of π or 0, the phase difference $\Delta\varphi_{PB}$ can be assumed to be φ_{2PB} based on Bloch theory [20]. For the integrity of rotatory nonlinear optical theory, the periodic step functions of φ_{1PB} and φ_{2PB} should be discussed and expressed as

$$\varphi_{1PB} = \begin{cases} 0, & 2aL_1 \leqslant r < (2a+1)L_1 \\ \pi, & (2a+1)L_1 \leqslant r < (2a+2)L_1 \end{cases},$$
$$a = 0, \ 1, \ 2, \ 3 \ldots \quad (20)$$

$$\varphi_{2PB} = \begin{cases} 0, & 2aL_2 \leqslant r < (2a+1)L_2 \\ \pi, & (2a+1)L_2 \leqslant r < (2a+2)L_2 \end{cases},$$
$$a = 0, \ 1, \ 2, \ 3 \ldots \quad (21)$$

where L_1 and L_2, defined as $L_1 = \pi/\rho_1$ and $L_2 = \pi/\rho_2$, are the propagation lengths in the crystal that allow for the generation of a PB phase of π in the fundamental and SH waves, respectively, and a is a non-negative integer. If PB phases are introduced, the phase terms in $\vec{E}^{\omega}$ and $\vec{E}^{2\omega}$ will have an additional step function of φ_{1PB} and φ_{2PB}, where φ_{1PB} and φ_{2PB} are the added PB phases of the fundamental and SH waves, respectively. Then, $\vec{E}^{\omega}(r)$, $\vec{E}^{2\omega}(r)$, and $\vec{P}_{\text{eff}}^{2\omega}(r)$ become

$$\vec{E}_1'(r) = \vec{A}^{\omega} e^{-i(\omega t - k_1 r + \varphi_{1PB})}, \quad (22)$$

$$\vec{E}_2'(r) = \vec{A}^{2\omega'} e^{-i(2\omega t - k_2 r + \varphi_{2PB})}, \quad (23)$$

$$\vec{P}_{\text{eff}}^{2\omega'}(r) = \varepsilon_0 \vec{d}_{\text{eff}}(r)|\vec{A}^{\omega}|^2 e^{-2i(\omega t - k_1 r + \varphi_{1PB})}. \quad (24)$$

Considering that the value of the step function φ_{1PB} doubled is equivalent to zero, only φ_{2PB} is added to the phase of the coupling wave equation, which can be expressed as

$$\frac{d\vec{A}^{2\omega'}}{dr} = \frac{\pi i \vec{d}_{\text{eff}}(r)|\vec{A}^{\omega}|^2}{n_2 \lambda} e^{i(\Delta kr + \varphi_{2PB})}. \quad (25)$$

The term $\exp(i\,\varphi_{2PB})$ is a step function of length r, as shown in Fig. 2(d). Using the Fourier transform to decompose the right-hand side of Eq. (25) and considering only the odd mth-order terms, a coupled-amplitude equation for SHG in rotatory crystals is obtained as

$$\frac{d\vec{A}^{2\omega'}}{dr} = -\frac{\pi \vec{d}_{\text{eff}}(r)|\vec{A}^{\omega}|^2}{n_2 \lambda} \frac{2}{m\pi} e^{i\Delta k_Q r}, \ m = \pm 1, \pm 3, \pm 5, \ldots,$$
$$(26)$$

where the wave-vector mismatch for the mth-order QPM is given by $\Delta k_Q = 2k_1 - k_2 + m\rho_2$, $m\rho_2$ can be assumed as the "grating wave vector" in QPM, and the sign of m depends on that of Δk. By analyzing Eqs. (7) and (26), the PM conditions involving PB phases can be inferred as $\Delta k_Q \pm \rho_2 = 0$, $\Delta k_Q \pm (2\rho_1 - \rho_2) = 0$, and $\Delta k_Q \pm (2\rho_1 + \rho_2) = 0$. Furthermore, the analysis shows that ρ_2 plays a more important role in the rotation QPM compared with ρ_1, and $2\rho_1$ is usually lower than ρ_2, considering the dispersion of optical rotation. If $2\rho_1$ is much less than $(m \pm 1)\rho_2$, meaning that it can be neglected, the PM conditions can be simplified to $\Delta k + (m \pm 1)\rho_2 = 0$. Equations (9)–(11) then become

$$A_1^{2\omega'} = -\frac{\pi |\vec{A}^{\omega}|^2}{n_2 \lambda} \frac{2}{m\pi} \left\{ \frac{e^{i[\Delta k + (m-1)\rho_2]L} - 1}{\Delta k + (m-1)\rho_2}(X_1 + X_4 + X_5)e^{i\rho_2 L} \right.$$
$$\left. + \frac{e^{i[\Delta k + (m+1)\rho_2]L} - 1}{\Delta k + (m+1)\rho_2}(X_2 + X_3 + X_6)e^{-i\rho_2 L} \right\}, \quad (27)$$

$$A_2^{2\omega'} = -\frac{\pi |\vec{A}^{\omega}|^2}{n_2 \lambda} \frac{2}{m\pi} \left\{ \frac{e^{i[\Delta k + (m-1)\rho_2]L} - 1}{\Delta k + (m-1)\rho_2}(Y_1 + Y_4 + Y_5)e^{i\rho_2 L} \right.$$
$$\left. + \frac{e^{i[\Delta k + (m+1)\rho_2]L} - 1}{\Delta k + \rho_2}(Y_2 + Y_3 + Y_6)e^{-i\rho_2 L} \right\}, \quad (28)$$
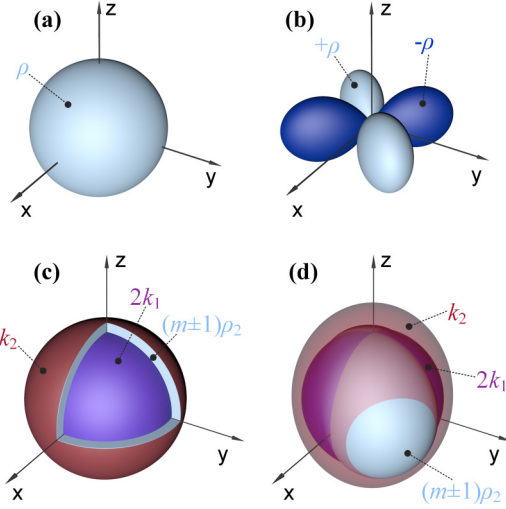
FIG. 3. Schematic of (a) rotatory power of cubic crystals (class of 432 and 23), (b) rotatory power of birefringent crystals (class of $\bar{4}2m$ and $mm2$), (c) rotation QPM in cubic crystals, and (d) rotation QPM in birefringent crystals. The gray (light gray) and blue (dark gray) regions represent the rotatory power but are of opposite signs. The partial deletion of spheres in (c) is plotted for the exhibition of the inside. The red (outer) and purple (inner) spheres in (c) and (d) represent the wave vector of $2k_1$ and k_2. Optical rotation can contribute to the PM and connect the surface of $2k_1$ and k_2. The intersection of $2k_1 + (m \pm 1)\rho_2$ (purple and gray) and k_2 (red) in (d) represents the PM orientation.

$$A_3^{2\omega'} = -\frac{\pi |\vec{A}^\omega|^2}{n_2 \lambda} \frac{2}{m\pi} \left\{ \frac{e^{i[\Delta k + (m-1)\rho_2]L} - 1}{\Delta k + (m-1)\rho_2} (Z_1 + Z_4 + Z_5) e^{i\rho_2 L} \right.$$
$$\left. + \frac{e^{i[\Delta k + (m+1)\rho_2]L} - 1}{\Delta k + (m+1)\rho_2} (Z_2 + Z_3 + Z_6) e^{-i\rho_2 L} \right\}. \quad (29)$$

Obviously, if there is no rotation in the nonlinear crystal, that is, $\rho_1 = \rho_2 = 0$, Eqs. (27)–(29) agree exactly with the results of the SHG without rotation. The above results of the rotation QPM conditions for SHG cannot only be applied to the groups 23 and $\bar{4}3m$ but also to all 20 acentric point groups. The only difference among the different point groups are the factors X_i, Y_i, and Z_i, which result from the different second-order susceptibility tensors. Correspondingly, the relative intensity and conversion efficiency of the output SH radiation, taking into account the PB phases, are given by

$$I'_\pm \propto \left(\frac{2}{m}\right)^2 I_1{}^2 \mathrm{sinc}^2\left(\frac{\Delta k_\pm L}{2}\right) L^2 (X_\pm X_\pm^* + Y_\pm Y_\pm^* + Z_\pm Z_\pm^*), \quad (30)$$

where $\Delta k_\pm = \Delta k + (m \pm 1)\rho_2$, and $X_+ = X_2 + X_3 + X_6$, $X_- = X_1 + X_4 + X_5$, $Y_+ = Y_2 + Y_3 + Y_6$, $Y_- = Y_1 + Y_4 + Y_5$, $Z_+ = Z_2 + Z_3 + Z_6$, and $Z_- = Z_1 + Z_4 + Z_5$. If $\Delta k_\pm = 0$, the corresponding maximum conversion efficiency is

$$\eta'_{\pm\max} = \frac{4|\vec{A}^\omega|^2}{mn_1 n_2 \lambda^2} L^2 (X_\pm X_\pm^* + Y_\pm Y_\pm^* + Z_\pm Z_\pm^*). \quad (31)$$

This analysis shows that the optical rotation of waves can compensate for the phase mismatch in SHG. The QPM in the rotatory crystals is shown schematically in Fig. 3. The PB and
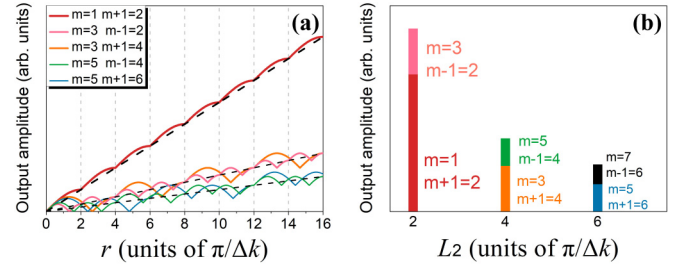

FIG. 4. (a) Amplitude of the SH wave as a function of the propagation length r under the 1-, 3-, and 5-order QPM conditions with a wave-vector mismatch of Δk. (b) Amplitude of the SH waves under propagation length $L_2 = 2\pi/\Delta k$, $4\pi/\Delta k$, and $6\pi/\Delta k$.

rotation phases can work together during QPM. Figures 3(a) and 3(b) show two types of schematic rotatory power, and the summation of $2k_1$ and $(m \pm 1)\rho_2$ could intersect with k_2, as shown in Figs. 3(c) and 3(d). Note that the optical rotation power of birefringent crystals is not a scalar, as shown in Fig. 3(b). Therefore, the value of ρ is associated with gyration tensor of the corresponding crystal. The contributions of the PB phases and the rotation to the QPM were $m\rho_2$ and $\pm\rho_2$, respectively. They provide a function for filling the gap of the wave-vector mismatch, Δk, for SHG. With a mismatched wave vector, Δk, the amplitudes of the output SH waves for the 1-, 3-, and 5-order QPMs are shown in Fig. 4(a) as a function of r. If the period L_2 is sufficient, the other orders can be neglected, and the curves can be approximately linear with length r [see dotted line in Fig. 4(a)]. The conditions of $m - 1$ and $m + 1$ for the mth order have the same gain, although the conditions $m - 1$ and $m + 1$ have different values of L_2, corresponding to a different ρ_2. The conditions of $m = 3$ with $m + 1 = 4$ and $m = 5$ with $m - 1 = 4$ have the same value of L_2, which means that the two conditions can be achieved simultaneously. The summed output amplitudes for different L_2 values are shown in Fig. 4(b).

According to the higher-order Poincaré sphere and the higher-order PB phase for vectorial vortex beams [14], the higher-order PB phase is given by $\varphi_{HPB} = (\pm l + l)\varphi_{PB}$, where l is the topological charge corresponding to the orbital angular momentum. Considering the angular momentum conversion [21], the topological charge of the SH wave is $2l$ for the case of the fundamental vortex with a topological charge l. Therefore, the periodically added PB phases of the fundamental and SH waves are expressed as $(\pm l + l)\pi$ and $(\pm 2l + l)\pi$, respectively. The double higher-order PB phase of the fundamental wave, $2(\pm l + l)\pi$, can also be reduced to zero, and the higher-order PB phase, $(\pm 2l + l)\pi$, equals π. Therefore, in SHG, the orbital angular momentum has no modulation of the PM.

V. DISCUSSION

Table I provides a comparison of the natural rotatory power and the phase mismatching in the orientation of the maximum rotatory power for several optically active crystals. Unfortunately, it is difficult to compensate for the typical phase mismatch, although some crystals possess a large optical rotatory power. To achieve rotation QPM, magneto-optical

TABLE I. Phase mismatch and rotatory power of typical nonlinear or optical activity crystals.

Crystal	Point group	Orientation of maximum rotatory power	Phase mismatch in this orientation @2ω (°/mm)	Rotatory power (°/mm)	Ref.
$CsLiB_6O_{10}$ (CLBO)	$\bar{4}2m$	$\theta = 90°$, $\psi = 45°$	22 835.7@633 nm	19@633 nm	[26,27]
KH_2PO_4 (KDP)	$\bar{4}2m$	$\theta = 90°$, $\psi = 45°$	4 792.8 @633 nm	7.42@633 nm	[28,29]
$KTiOPO_4$ (KTP)	$mm2$	$\theta = 90°$, $\psi = 45°$	16 931.6@633 nm	20.5@633 nm	[30,31]
$La_3Ga_{5.5}Nb_{0.5}O_{14}$ (LGN)	32	$\theta = 0°$	25 688@532 nm	~27@532 nm	[32,33]
$AgGaS_2$ (AGS)	$\bar{4}2m$	$\theta = 90°$, $\psi = 45°$	97 086.3 @532 nm	~250@532 nm	[34,35]
$CdSiP_2$ (CSP)	$\bar{4}2m$	$\theta = 90°$, $\psi = 45°$	25 331.8@800 nm	~155@800 nm	[36,37]
$ZnGeP_2$ (ZGP)	$\bar{4}2m$	$\theta = 90°$, $\psi = 45°$	28 241.5 @1064 nm	~68@1064 nm	[36,38]
$Bi_{12}GeO_{20}$ (BGO)	23	Isotropy	12 0413 @532 nm	~35@532 nm	[39,40]

materials with large Faraday rotations are required. It has also been found that $Bi_3Fe_5O_{12}$ films show a high Faraday rotation over $2 \times 10^{4°}$/mm at ~530 nm under a magnetic field of 120 mT [22], corresponding to length $L_2 = 9\,\mu m$ for the generation of a PB phase π. This is of the same order of magnitude as the typical grating period of periodically poled lithium niobate [23] and can compensate for the wavevector mismatch of ~$4 \times 10^{4°}$/mm, ~$8 \times 10^{4°}$/mm, and ~$12 \times 10^{4°}$/mm corresponding to $|m \pm 1| = 2$, $|m \pm 1| = 4$, $|m \pm 1| = 6$, respectively. In contrast to the periodic polarization QPM, the length of the period in rotation QPM is determined by the rotation velocity of the linear polarization plane. Considering the dependence on the applied magnetic field, the QPM conditions are more flexible for tunable wavelength generation as compared to the traditional PM. Associated with the Faraday rotation applied in optical and quantum chips [24,25], the proposed QPM conditions could give rise to nonlinear optics to further develop modern optics on chips.

In conclusion, the QPM conditions in rotatory nonlinear optics were theoretically presented, which indicated that PB topological phases can be employed to compensate for mismatched phases in SHG. Compared with the previous work [9], we do not only extend the PM results in this to general cases, but also introduce the PB phases to QPM which should be more flexible in further application. The possible QPM conditions were then analyzed and calculated. It is believed that the proposed QPM conditions in rotatory nonlinear optics should be universal and could have promising applications in modern optoelectronics and photonics, especially in chip optics with Faraday rotation and nonlinear frequency conversions.

APPENDIX A: EFFECTIVE NONLINEAR COEFFICIENT IN CUBIC NONLINEAR CRYSTAL

$$\vec{d}_{\mathrm{eff}}(r) = \begin{pmatrix} [\vec{d}_{\mathrm{eff}}(r)]_1 \\ [\vec{d}_{\mathrm{eff}}(r)]_2 \\ [\vec{d}_{\mathrm{eff}}(r)]_3 \end{pmatrix}, \tag{A1}$$

where $[\vec{d}_{\mathrm{eff}}(r)]_1$, $[\vec{d}_{\mathrm{eff}}(r)]_2$, and $[\vec{d}_{\mathrm{eff}}(r)]_3$ represent the components of $\vec{d}_{\mathrm{eff}}(r)$ along the x-, y-, and z axes, respectively, given by

$$\begin{aligned}
[\vec{d}_{\mathrm{eff}}(r)]_1 = d_{14}\Big(&-\sin\alpha_2 \sin\theta(\cos\theta\cos\psi\sin\alpha_1 + \cos\alpha_1\sin\psi)(\cos\theta(-3 + \cos2\psi)\sin\alpha_1 + \cos\alpha_1\sin2\psi) \\
&+ \tfrac{1}{16}\cos\alpha_2\sin\theta(16\cos\psi(1 + \cos2\theta\cos2\psi)\sin2\alpha_1 + ((-13 + 21\cos2\alpha_1)\cos\theta - 6\cos3\theta\sin^2\alpha_1)\sin\psi \\
&+ 2\cos\theta(3 + \cos2\alpha_1 - 6\cos2\theta\sin^2\alpha_1)\sin3\psi)\Big),
\end{aligned} \tag{A2}$$

$$[\vec{d}_{\text{eff}}(r)]_2 = d_{14}\big(\tfrac{1}{16}\sin\theta(\cos\alpha_2(-3\cos 3\theta\cos\psi + \cos\theta((-13 + 6\cos 2\alpha_1(3 + \cos 2\theta))\cos\psi$$
$$- 2\cos 3\psi(3 + \cos 2\alpha_1 - 6\cos 2\theta\sin^2\alpha_1)) + 16(-1 + \cos 2\theta\cos 2\psi)\sin 2\alpha_1\sin\psi)$$
$$+ 2\sin\alpha_2(16\cos\theta\cos^3\psi\sin 2\alpha_1 + (-3 + 7\cos 2\alpha_1)\sin\psi + (1 + 3\cos\alpha_1)\sin 3\psi$$
$$- 2\cos 2\theta\sin^2\alpha_1(5\sin\psi + \sin 3\psi)))\big), \tag{A3}$$

$$[\vec{d}_{\text{eff}}(r)]_3 = d_{14}\big(2\sin^2\theta(-(-1 + \cos\alpha_2)\cos\theta\cos\psi - \sin\alpha_2\sin\psi)(\cos^2\theta\cos^3\psi\sin 2\alpha_1$$
$$+ \cos^2\alpha_1\cos\theta\cos^2\psi\sin\psi + \tfrac{1}{2}\sin\alpha_1\sin\psi(-\cos^3\theta(3 + \cos 2\psi)\sin\alpha_1$$
$$+ 2\cos\theta\cos 2\psi\sin\alpha_1\sin^2\theta + 4\cos\alpha_1\cos\psi\sin^2\theta\sin\psi)) - \tfrac{1}{2}\sin^2\theta(\cos\psi\sin\alpha_2$$
$$- (\cos\alpha_2 - 1)\cos\theta\sin\psi)(4\cos^2\psi\sin 2\alpha_1\sin^2\theta\sin\psi + 4\cos^2\theta\sin 2\alpha_1\sin^3\psi$$
$$+ \cos\theta(((4 + \cos 2\theta)\cos\psi - \cos 2\theta\cos 3\psi)\sin^2\alpha_1 - 4\cos\psi(\cos^2\alpha_1 + \sin^2\alpha_1\sin^2\theta)\sin^2\psi)) - \tfrac{1}{4}(\cos^2\theta$$
$$+ \cos\alpha_2\sin^2\theta)(8\cos\theta\cos 2\psi\sin 2\alpha_1\sin^2\theta + 8\cos^2\alpha_1\cos\psi\sin\psi + \cos^2\theta(-5 + \cos 2\alpha_1$$
$$+ 6\cos 2\theta\sin^2\alpha_1)\sin 2\psi)\big). \tag{A4}$$

APPENDIX B: EXPRESSIONS OF X_i, Y_i, AND Z_i

$$X_1 = -\tfrac{1}{256}id_{14}e^{-i(4\theta+3\psi)}(e^{2i\theta} - 1)[-3 + 2e^{i\theta} + 3e^{2i\theta} - 4e^{3i\theta} + 3e^{4i\theta} + 2e^{5i\theta} - 3e^{6i\theta} - 12e^{3i\theta+2i\psi}$$
$$- 10e^{5i\theta+2i\psi} - 12e^{3i\theta+4i\psi} - 10e^{5i\theta+4i\psi} + 3e^{6i\theta+4i\psi} - 3e^{4i\theta+6i\psi} + 2e^{5i\theta+6i\psi} - 3e^{2i\psi} + 3e^{4i\psi} + 3e^{6i\psi}$$
$$- 13e^{2i(\theta+\psi)} + 13e^{4i(\theta+\psi)} + 3e^{6i(\theta+\psi)} - 13e^{2i(2\theta+\psi)} - 3e^{2i(3\theta+\psi)} - 10e^{i(\theta+2\psi)} + 13e^{2i(\theta+2\psi)}$$
$$- 4e^{3i(\theta+2\psi)} - 3e^{2i(\theta+3\psi)} - 10e^{i(\theta+4\psi)} + 2e^{i(\theta+6\psi)}], \tag{B1}$$

$$X_2 = -\tfrac{1}{256}id_{14}e^{-i(4\theta+3\psi)}(e^{2i\theta} - 1)[-3 - 2e^{i\theta} + 3e^{2i\theta} + 4e^{3i\theta} + 3e^{4i\theta} - 2e^{5i\theta} - 3e^{6i\theta} + 12e^{3i\theta+2i\psi}$$
$$+ 10e^{5i\theta+2i\psi} + 12e^{3i\theta+4i\psi} + 10e^{5i\theta+4i\psi} + 3e^{6i\theta+4i\psi} - 3e^{4i\theta+6i\psi} - 2e^{5i\theta+6i\psi} - 3e^{2i\psi} + 3e^{4i\psi} + 3e^{6i\psi}$$
$$- 13e^{2i(\theta+\psi)} + 13e^{4i(\theta+\psi)} + 3e^{6i(\theta+\psi)} - 13e^{2i(2\theta+\psi)} - 3e^{2i(3\theta+\psi)} + 10e^{i(\theta+2\psi)} + 13e^{2i(\theta+2\psi)}$$
$$+ 4e^{3i(\theta+2\psi)} - 3e^{2i(\theta+3\psi)} + 10e^{i(\theta+4\psi)} - 2e^{i(\theta+6\psi)}], \tag{B2}$$

$$X_3 = \tfrac{1}{512}id_{14}e^{-i(4\theta+3\psi)}(e^{2i\theta} - 1)[-3 - 10e^{i\theta} - 13e^{2i\theta} - 12e^{3i\theta} - 13e^{4i\theta} - 10e^{5i\theta} - 3e^{6i\theta}$$
$$- 4e^{3i\theta+2i\psi} + 2e^{5i\theta+2i\psi} - 4e^{3i\theta+4i\psi} + 2e^{5i\theta+4i\psi} + 3e^{6i\theta+4i\psi} + 13e^{4i\theta+6i\psi} - 10e^{5i\theta+6i\psi} - 3e^{2i\psi}$$
$$+ 3e^{4i\psi} + 3e^{6i\psi} + 3e^{2i(\theta+\psi)} - 3e^{4i(\theta+\psi)} + 3e^{6i(\theta+\psi)} + 3e^{2i(2\theta+\psi)} - 3e^{2i(3\theta+\psi)} + 2e^{i(\theta+2\psi)}$$
$$- 3e^{2i(\theta+2\psi)} - 12e^{3i(\theta+2\psi)} + 13e^{2i(\theta+3\psi)} + 2e^{i(\theta+4\psi)} - 10e^{i(\theta+6\psi)}], \tag{B3}$$

$$X_4 = \tfrac{1}{512}id_{14}e^{-i(4\theta+3\psi)}(e^{2i\theta} - 1)[-3 + 10e^{i\theta} - 13e^{2i\theta} + 12e^{3i\theta} - 13e^{4i\theta} + 10e^{5i\theta} - 3e^{6i\theta}$$
$$+ 4e^{3i\theta+2i\psi} - 2e^{5i\theta+2i\psi} + 4e^{3i\theta+4i\psi} - 2e^{5i\theta+4i\psi} + 3e^{6i\theta+4i\psi} + 13e^{4i\theta+6i\psi} + 10e^{5i\theta+6i\psi} - 3e^{2i\psi}$$
$$+ 3e^{4i\psi} + 3e^{6i\psi} + 3e^{2i(\theta+\psi)} - 3e^{4i(\theta+\psi)} + 3e^{6i(\theta+\psi)} + 3e^{2i(2\theta+\psi)} - 3e^{2i(3\theta+\psi)} - 2e^{i(\theta+2\psi)}$$
$$- 3e^{2i(\theta+2\psi)} + 12e^{3i(\theta+2\psi)} + 13e^{2i(\theta+3\psi)} - 2e^{i(\theta+4\psi)} + 10e^{i(\theta+6\psi)}], \tag{B4}$$

$$X_5 = \tfrac{3}{512}id_{14}e^{-i(4\theta+3\psi)}(e^{2i\theta} - 1)[-1 - 2e^{i\theta} + e^{2i\theta} + 4e^{3i\theta} + e^{4i\theta} - 2e^{5i\theta} - e^{6i\theta} - 20e^{3i\theta+2i\psi}$$
$$- 6e^{5i\theta+2i\psi} - 20e^{3i\theta+4i\psi} - 6e^{5i\theta+4i\psi} + e^{6i\theta+4i\psi} - e^{4i\theta+6i\psi} - 2e^{5i\theta+6i\psi} - e^{2i\psi} + e^{4i\psi} + e^{6i\psi}$$
$$- 15e^{2i(\theta+\psi)} + 15e^{4i(\theta+\psi)} + e^{6i(\theta+\psi)} - 15e^{2i(2\theta+\psi)} - e^{2i(3\theta+\psi)} - 6e^{i(\theta+2\psi)} + 15e^{2i(\theta+2\psi)} + 4e^{3i(\theta+2\psi)}$$
$$- e^{2i(\theta+3\psi)} - 6e^{i(\theta+4\psi)} - 2e^{i(\theta+6\psi)}], \tag{B5}$$

$$X_6 = \tfrac{3}{512} i d_{14} e^{-i(4\theta+3\psi)}(e^{2i\theta}-1)[-1 + 2e^{i\theta} + e^{2i\theta} - 4e^{3i\theta} + e^{4i\theta} + 2e^{5i\theta} - e^{6i\theta} + 20e^{3i\theta+2i\psi}$$
$$+ 6e^{5i\theta+2i\psi} + 20e^{3i\theta+4i\psi} + 6e^{5i\theta+4i\psi} + e^{6i\theta+4i\psi} - e^{4i\theta+6i\psi} + 2e^{5i\theta+6i\psi} - e^{2i\psi} + e^{4i\psi} + e^{6i\psi}$$
$$- 15e^{2i(\theta+\psi)} + 15e^{4i(\theta+\psi)} + e^{6i(\theta+\psi)} - 15e^{2i(2\theta+\psi)} - e^{2i(3\theta+\psi)} + 6e^{i(\theta+2\psi)} + 15e^{2i(\theta+2\psi)} - 4e^{3i(\theta+2\psi)}$$
$$- e^{2i(\theta+3\psi)} + 6e^{i(\theta+4\psi)} + 2e^{i(\theta+6\psi)}] . \tag{B6}$$

$$Y_1 = -\tfrac{1}{256} d_{14} e^{-i(4\theta+3\psi)}(e^{2i\theta}-1)[3 - 2e^{i\theta} - 3e^{2i\theta} + 4e^{3i\theta} - 3e^{4i\theta} - 2e^{5i\theta} + 3e^{6i\theta} - 12e^{3i\theta+2i\psi}$$
$$- 10e^{5i\theta+2i\psi} + 12e^{3i\theta+4i\psi} + 10e^{5i\theta+4i\psi} - 3e^{6i\theta+4i\psi} - 3e^{4i\theta+6i\psi} + 2e^{5i\theta+6i\psi} - 3e^{2i\psi} - 3e^{4i\psi} + 3e^{6i\psi}$$
$$- 13e^{2i(\theta+\psi)} - 13e^{4i(\theta+\psi)} + 3e^{6i(\theta+\psi)} - 13e^{2i(2\theta+\psi)} - 3e^{2i(3\theta+\psi)} - 10e^{i(\theta+2\psi)} - 13e^{2i(\theta+2\psi)}$$
$$- 4e^{3i(\theta+2\psi)} - 3e^{2i(\theta+3\psi)} + 10e^{i(\theta+4\psi)} + 2e^{i(\theta+6\psi)}], \tag{B7}$$

$$Y_2 = -\tfrac{1}{256} d_{14} e^{-i(4\theta+3\psi)}(e^{2i\theta}-1)[3 + 2e^{i\theta} - 3e^{2i\theta} - 4e^{3i\theta} - 3e^{4i\theta} + 2e^{5i\theta} + 3e^{6i\theta} + 12e^{3i\theta+2i\psi}$$
$$+ 10e^{5i\theta+2i\psi} - 12e^{3i\theta+4i\psi} - 10e^{5i\theta+4i\psi} - 3e^{6i\theta+4i\psi} - 3e^{4i\theta+6i\psi} - 2e^{5i\theta+6i\psi} - 3e^{2i\psi} - 3e^{4i\psi} + 3e^{6i\psi}$$
$$- 13e^{2i(\theta+\psi)} - 13e^{4i(\theta+\psi)} + 3e^{6i(\theta+\psi)} - 13e^{2i(2\theta+\psi)} - 3e^{2i(3\theta+\psi)} + 10e^{i(\theta+2\psi)} - 13e^{2i(\theta+2\psi)}$$
$$+ 4e^{3i(\theta+2\psi)} - 3e^{2i(\theta+3\psi)} - 10e^{i(\theta+4\psi)} - 2e^{i(\theta+6\psi)}], \tag{B8}$$

$$Y_3 = \tfrac{1}{512} d_{14} e^{-i(4\theta+3\psi)}(e^{2i\theta}-1)[3 + 10e^{i\theta} + 13e^{2i\theta} + 12e^{3i\theta} + 13e^{4i\theta} + 10e^{5i\theta} + 3e^{6i\theta} - 4e^{3i\theta+2i\psi}$$
$$+ 2e^{5i\theta+2i\psi} + 4e^{3i\theta+4i\psi} - 2e^{5i\theta+4i\psi} - 3e^{6i\theta+4i\psi} + 13e^{4i\theta+6i\psi} - 10e^{5i\theta+6i\psi} - 3e^{2i\psi} - 3e^{4i\psi} + 3e^{6i\psi}$$
$$+ 3e^{2i(\theta+\psi)} + 3e^{4i(\theta+\psi)} + 3e^{6i(\theta+\psi)} + 3e^{2i(2\theta+\psi)} - 3e^{2i(3\theta+\psi)} + 2e^{i(\theta+2\psi)} + 3e^{2i(\theta+2\psi)} - 12e^{3i(\theta+2\psi)}$$
$$+ 13e^{2i(\theta+3\psi)} - 2e^{i(\theta+4\psi)} - 10e^{i(\theta+6\psi)}], \tag{B9}$$

$$Y_4 = \tfrac{1}{512} d_{14} e^{-i(4\theta+3\psi)}(e^{2i\theta}-1)[3 - 10e^{i\theta} + 13e^{2i\theta} - 12e^{3i\theta} + 13e^{4i\theta} - 10e^{5i\theta} + 3e^{6i\theta} + 4e^{3i\theta+2i\psi}$$
$$- 2e^{5i\theta+2i\psi} - 4e^{3i\theta+4i\psi} + 2e^{5i\theta+4i\psi} - 3e^{6i\theta+4i\psi} + 13e^{4i\theta+6i\psi} + 10e^{5i\theta+6i\psi} - 3e^{2i\psi} - 3e^{4i\psi} + 3e^{6i\psi}$$
$$+ 3e^{2i(\theta+\psi)} + 3e^{4i(\theta+\psi)} + 3e^{6i(\theta+\psi)} + 3e^{2i(2\theta+\psi)} - 3e^{2i(3\theta+\psi)} - 2e^{i(\theta+2\psi)} + 3e^{2i(\theta+2\psi)} + 12e^{3i(\theta+2\psi)}$$
$$+ 13e^{2i(\theta+3\psi)} + 2e^{i(\theta+4\psi)} + 10e^{i(\theta+6\psi)}], \tag{B10}$$

$$Y_5 = \tfrac{3}{512} d_{14} e^{-i(4\theta+3\psi)}(e^{2i\theta}-1)[1 + 2e^{i\theta} - e^{2i\theta} - 4e^{3i\theta} - e^{4i\theta} + 2e^{5i\theta} + e^{6i\theta} - 20e^{3i\theta+2i\psi}$$
$$- 6e^{5i\theta+2i\psi} + 20e^{3i\theta+4i\psi} + 6e^{5i\theta+4i\psi} - e^{6i\theta+4i\psi} - e^{4i\theta+6i\psi} - 2e^{5i\theta+6i\psi} - e^{2i\psi} - e^{4i\psi} + e^{6i\psi}$$
$$- 15e^{2i(\theta+\psi)} - 15e^{4i(\theta+\psi)} + e^{6i(\theta+\psi)} - 15e^{2i(2\theta+\psi)} - e^{2i(3\theta+\psi)} - 6e^{i(\theta+2\psi)} - 15e^{2i(\theta+2\psi)} + 4e^{3i(\theta+2\psi)}$$
$$- e^{2i(\theta+3\psi)} + 6e^{i(\theta+4\psi)} - 2e^{i(\theta+6\psi)}], \tag{B11}$$

$$Y_6 = \tfrac{3}{512} d_{14} e^{-i(4\theta+3\psi)}(e^{2i\theta}-1)[1 - 2e^{i\theta} - e^{2i\theta} + 4e^{3i\theta} - e^{4i\theta} - 2e^{5i\theta} + e^{6i\theta} + 20e^{3i\theta+2i\psi}$$
$$+ 6e^{5i\theta+2i\psi} - 20e^{3i\theta+4i\psi} - 6e^{5i\theta+4i\psi} - e^{6i\theta+4i\psi} - e^{4i\theta+6i\psi} + 2e^{5i\theta+6i\psi} - e^{2i\psi} - e^{4i\psi} + e^{6i\psi}$$
$$- 15e^{2i(\theta+\psi)} - 15e^{4i(\theta+\psi)} + e^{6i(\theta+\psi)} - 15e^{2i(2\theta+\psi)} - e^{2i(3\theta+\psi)} + 6e^{i(\theta+2\psi)} - 15e^{2i(\theta+2\psi)} - 4e^{3i(\theta+2\psi)}$$
$$- e^{2i(\theta+3\psi)} - 6e^{i(\theta+4\psi)} + 2e^{i(\theta+6\psi)}]. \tag{B12}$$

$$Z_1 = \tfrac{1}{128} d_{14} e^{-2i(2\theta+\psi)}(e^{2i\theta}-1)^2[-3 - 4e^{i\theta} - 2e^{2i\theta} - 4e^{3i\theta} - 3e^{4i\theta}$$
$$- 4e^{3i\theta+4i\psi} + 3e^{4i\psi} + 3e^{4i(\theta+\psi)} + 2e^{2i(\theta+2\psi)} - 4e^{i(\theta+4\psi)}], \tag{B13}$$

$$Z_2 = \tfrac{1}{128} d_{14} e^{-2i(2\theta+\psi)}(e^{2i\theta}-1)^2[-3 + 4e^{i\theta} - 2e^{2i\theta} + 4e^{3i\theta} - 3e^{4i\theta}$$
$$+ 4e^{3i\theta+4i\psi} + 3e^{4i\psi} + 3e^{4i(\theta+\psi)} + 2e^{2i(\theta+2\psi)} + 4e^{i(\theta+4\psi)}], \tag{B14}$$

$$Z_3 = -\tfrac{1}{256} d_{14} e^{-2i(2\theta+\psi)}(e^{2i\theta}-1)^2[-3 - 4e^{i\theta} - 2e^{2i\theta} - 4e^{3i\theta} - 3e^{4i\theta} - 4e^{3i\theta+4i\psi}$$
$$+ 3e^{4i\psi} + 3e^{4i(\theta+\psi)} + 2e^{2i(\theta+2\psi)} - 4e^{i(\theta+4\psi)}], \tag{B15}$$

$$Z_4 = -\frac{1}{256}d_{14}e^{-2i(2\theta+\psi)}(e^{2i\theta}-1)^2[-3+4e^{i\theta}-2e^{2i\theta}+4e^{3i\theta}-3e^{4i\theta}+4e^{3i\theta+4i\psi}$$
$$+3e^{4i\psi}+3e^{4i(\theta+\psi)}+2e^{2i(\theta+2\psi)}+4e^{i(\theta+4\psi)}], \tag{B16}$$

$$Z_5 = -\frac{3}{256}d_{14}e^{-2i(2\theta+\psi)}(e^{2i\theta}-1)^2[-1-4e^{i\theta}-6e^{2i\theta}-4e^{3i\theta}-e^{4i\theta}$$
$$-4e^{3i\theta+4i\psi}+e^{4i\psi}+e^{4i(\theta+\psi)}+6e^{2i(\theta+2\psi)}-4e^{i(\theta+4\psi)}], \tag{B17}$$

$$Z_6 = -\frac{3}{256}d_{14}e^{-2i(2\theta+\psi)}(e^{2i\theta}-1)^2[-1+4e^{i\theta}-6e^{2i\theta}+4e^{3i\theta}-e^{4i\theta}$$
$$+4e^{3i\theta+4i\psi}+e^{4i\psi}+e^{4i(\theta+\psi)}+6e^{2i(\theta+2\psi)}+4e^{i(\theta+4\psi)}]. \tag{B18}$$

APPENDIX C: RESULT FOR CRYSTALS BELONGING TO CLASS 32

A matrix of the second-order nonlinear optical coefficient for crystals belonging to point group 32, under the Kleinman symmetry condition, is shown [18]:

$$\begin{pmatrix} d_{11} & -d_{11} & 0 & 0 & 0 & 0 \\ 0 & 0 & 0 & 0 & 0 & -d_{11} \\ 0 & 0 & 0 & 0 & 0 & 0 \end{pmatrix}. \tag{C1}$$

Using the same derivation described above, the result of the complex amplitude of the output SH wave for the point group 32 is obtained. It has the same form of expression as in Eqs. (9)–(11), but different values of X_i, Y_i, and Z_i. X_i, Y_i, and Z_i are defined as

$$X_1 = -\frac{1}{256}id_{11}e^{-4i(\theta+\psi)}(e^{2i\theta}-1)^2[1-2e^{2i\theta}+e^{4i\theta}+4e^{3i\theta+2i\psi}+e^{4i\theta+6i\psi}+e^{2i\psi}+e^{6i\psi}+e^{8i\psi}$$
$$+6e^{2i(\theta+\psi)}+e^{2i(2\theta+\psi)}+4e^{i(\theta+2\psi)}-4e^{3i(\theta+2\psi)}+e^{4i(\theta+2\psi)}+6e^{2i(\theta+3\psi)}-2e^{2i(\theta+4\psi)}-4e^{i(\theta+6\psi)}], \tag{C2}$$

$$X_2 = -\frac{1}{256}id_{11}e^{-4i(\theta+\psi)}(e^{2i\theta}-1)^2[1-2e^{2i\theta}+e^{4i\theta}-4e^{3i\theta+2i\psi}+e^{4i\theta+6i\psi}+e^{2i\psi}+e^{6i\psi}+e^{8i\psi}$$
$$+6e^{2i(\theta+\psi)}+e^{2i(2\theta+\psi)}-4e^{i(\theta+2\psi)}+4e^{3i(\theta+2\psi)}+e^{4i(\theta+2\psi)}+6e^{2i(\theta+3\psi)}-2e^{2i(\theta+4\psi)}+4e^{i(\theta+6\psi)}], \tag{C3}$$

$$X_3 = \frac{1}{512}id_{11}e^{-4i(\theta+\psi)}(e^{2i\theta}-1)^2[1+4e^{i\theta}+6e^{2i\theta}+4e^{3i\theta}+e^{4i\theta}+e^{4i\theta+6i\psi}-4e^{3i\theta+8i\psi}+e^{2i\psi}+e^{6i\psi}+e^{8i\psi}-2e^{2i(\theta+\psi)}$$
$$+e^{2i(2\theta+\psi)}+e^{4i(\theta+2\psi)}-2e^{2i(\theta+3\psi)}+6e^{2i(\theta+4\psi)}-4e^{i(\theta+8\psi)}], \tag{C4}$$

$$X_4 = \frac{1}{512}id_{11}e^{-4i(\theta+\psi)}(e^{2i\theta}-1)^2[1-4e^{i\theta}+6e^{2i\theta}-4e^{3i\theta}+e^{4i\theta}+e^{4i\theta+6i\psi}+4e^{3i\theta+8i\psi}+e^{2i\psi}+e^{6i\psi}+e^{8i\psi}-2e^{2i(\theta+\psi)}$$
$$[3pt]+e^{2i(2\theta+\psi)}+e^{4i(\theta+2\psi)}-2e^{2i(\theta+3\psi)}+6e^{2i(\theta+4\psi)}+4e^{i(\theta+8\psi)}], \tag{C5}$$

$$X_5 = \frac{1}{512}id_{11}e^{-4i(\theta+\psi)}[1+4e^{i\theta}+4e^{2i\theta}-4e^{3i\theta}-10e^{4i\theta}-4e^{5i\theta}+4e^{6i\theta}+4e^{7i\theta}+e^{8i\theta}+56e^{3i\theta+2i\psi}$$
$$+56e^{5i\theta+2i\psi}+8e^{7i\theta+2i\psi}+70e^{4i\theta+6i\psi}-56e^{5i\theta+6i\psi}-8e^{7i\theta+6i\psi}+e^{8i\theta+6i\psi}+4e^{3i\theta+8i\psi}+4e^{5i\theta+8i\psi}$$
$$+4e^{6i\theta+8i\psi}-4e^{7i\theta+8i\psi}+e^{2i\psi}+e^{6i\psi}+e^{8i\psi}+28e^{2i(\theta+\psi)}+28e^{6i(\theta+\psi)}+e^{8i(\theta+\psi)}+70e^{2i(2\theta+\psi)}$$
$$+28e^{2i(3\theta+\psi)}+e^{2i(4\theta+\psi)}+8e^{i(\theta+2\psi)}-56e^{3i(\theta+2\psi)}-10e^{4i(\theta+2\psi)}+28e^{2i(\theta+3\psi)}+4e^{2i(\theta+4\psi)}$$
$$-8e^{i(\theta+6\psi)}-4e^{i(\theta+8\psi)}], \tag{C6}$$

$$X_6 = \frac{1}{512}id_{11}e^{-4i(\theta+\psi)}[1-4e^{i\theta}+4e^{2i\theta}+4e^{3i\theta}-10e^{4i\theta}+4e^{5i\theta}+4e^{6i\theta}-4e^{7i\theta}+e^{8i\theta}-56e^{3i\theta+2i\psi}$$
$$-56e^{5i\theta+2i\psi}-8e^{7i\theta+2i\psi}+70e^{4i\theta+6i\psi}+56e^{5i\theta+6i\psi}+8e^{7i\theta+6i\psi}+e^{8i\theta+6i\psi}-4e^{3i\theta+8i\psi}-4e^{5i\theta+8i\psi}$$
$$+4e^{6i\theta+8i\psi}+4e^{7i\theta+8i\psi}+e^{2i\psi}+e^{6i\psi}+e^{8i\psi}+28e^{2i(\theta+\psi)}+28e^{6i(\theta+\psi)}+e^{8i(\theta+\psi)}+70e^{2i(2\theta+\psi)}$$
$$+28e^{2i(3\theta+\psi)}+e^{2i(4\theta+\psi)}-8e^{i(\theta+2\psi)}+56e^{3i(\theta+2\psi)}-10e^{4i(\theta+2\psi)}+28e^{2i(\theta+3\psi)}+4e^{2i(\theta+4\psi)}$$
$$+8e^{i(\theta+6\psi)}+4e^{i(\theta+8\psi)}]. \tag{C7}$$

$$Y_1 = -\tfrac{1}{256}d_{11}e^{-4i(\theta+\psi)}(e^{2i\theta}-1)^2[-1+2e^{2i\theta}-e^{4i\theta}+4e^{3i\theta+2i\psi}-e^{4i\theta+6i\psi}+e^{2i\psi}-e^{6i\psi}+e^{8i\psi}$$
$$+6e^{2i(\theta+\psi)}+e^{2i(2\theta+\psi)}+4e^{i(\theta+2\psi)}+4e^{3i(\theta+2\psi)}+e^{4i(\theta+2\psi)}-6e^{2i(\theta+3\psi)}-2e^{2i(\theta+4\psi)}+4e^{i(\theta+6\psi)}], \tag{C8}$$

$$Y_2 = -\tfrac{1}{256}d_{11}e^{-4i(\theta+\psi)}(e^{2i\theta}-1)^2[-1+2e^{2i\theta}-e^{4i\theta}-4e^{3i\theta+2i\psi}-e^{4i\theta+6i\psi}+e^{2i\psi}-e^{6i\psi}+e^{8i\psi}$$
$$+6e^{2i(\theta+\psi)}+e^{2i(2\theta+\psi)}-4e^{i(\theta+2\psi)}-4e^{3i(\theta+2\psi)}+e^{4i(\theta+2\psi)}-6e^{2i(\theta+3\psi)}-2e^{2i(\theta+4\psi)}-4e^{i(\theta+6\psi)}], \tag{C9}$$

$$Y_3 = \tfrac{1}{512}d_{11}e^{-4i(\theta+\psi)}(e^{2i\theta}-1)^2[-1-4e^{i\theta}-6e^{2i\theta}-4e^{3i\theta}-e^{4i\theta}-e^{4i\theta+6i\psi}-4e^{3i\theta+8i\psi}+e^{2i\psi}-e^{6i\psi}+e^{8i\psi}-2e^{2i(\theta+\psi)}$$
$$+e^{2i(2\theta+\psi)}+e^{4i(\theta+2\psi)}+2e^{2i(\theta+3\psi)}+6e^{2i(\theta+4\psi)}-4e^{i(\theta+8\psi)}], \tag{C10}$$

$$Y_4 = \tfrac{1}{512}d_{11}e^{-4i(\theta+\psi)}(e^{2i\theta}-1)^2[-1+4e^{i\theta}-6e^{2i\theta}+4e^{3i\theta}-e^{4i\theta}-e^{4i\theta+6i\psi}+4e^{3i\theta+8i\psi}+e^{2i\psi}-e^{6i\psi}+e^{8i\psi}-2e^{2i(\theta+\psi)}$$
$$+e^{2i(2\theta+\psi)}+e^{4i(\theta+2\psi)}+2e^{2i(\theta+3\psi)}+6e^{2i(\theta+4\psi)}+4e^{i(\theta+8\psi)}], \tag{C11}$$

$$Y_5 = \tfrac{1}{512}d_{11}e^{-4i(\theta+\psi)}[-1-4e^{i\theta}-4e^{2i\theta}+4e^{3i\theta}+10e^{4i\theta}+4e^{5i\theta}-4e^{6i\theta}-4e^{7i\theta}-e^{8i\theta}+56e^{3i\theta+2i\psi}$$
$$+56e^{5i\theta+2i\psi}+8e^{7i\theta+2i\psi}-70e^{4i\theta+6i\psi}+56e^{5i\theta+6i\psi}+8e^{7i\theta+6i\psi}-e^{8i\theta+6i\psi}+4e^{3i\theta+8i\psi}+4e^{5i\theta+8i\psi}$$
$$+4e^{6i\theta+8i\psi}-4e^{7i\theta+8i\psi}+e^{2i\psi}-e^{6i\psi}+e^{8i\psi}+28e^{2i(\theta+\psi)}-28e^{6i(\theta+\psi)}+e^{8i(\theta+\psi)}+70e^{2i(2\theta+\psi)}$$
$$+28e^{2i(3\theta+\psi)}+e^{2i(4\theta+\psi)}+8e^{i(\theta+2\psi)}+56e^{3i(\theta+2\psi)}-10e^{4i(\theta+2\psi)}-28e^{2i(\theta+3\psi)}+4e^{2i(\theta+4\psi)}$$
$$+8e^{i(\theta+6\psi)}-4e^{i(\theta+8\psi)}], \tag{C12}$$

$$Y_6 = \tfrac{1}{512}d_{11}e^{-4i(\theta+\psi)}[-1+4e^{i\theta}-4e^{2i\theta}-4e^{3i\theta}+10e^{4i\theta}-4e^{5i\theta}-4e^{6i\theta}+4e^{7i\theta}-e^{8i\theta}-56e^{3i\theta+2i\psi}$$
$$-56e^{5i\theta+2i\psi}-8e^{7i\theta+2i\psi}-70e^{4i\theta+6i\psi}-56e^{5i\theta+6i\psi}-8e^{7i\theta+6i\psi}-e^{8i\theta+6i\psi}-4e^{3i\theta+8i\psi}-4e^{5i\theta+8i\psi}$$
$$+4e^{6i\theta+8i\psi}+4e^{7i\theta+8i\psi}+e^{2i\psi}-e^{6i\psi}+e^{8i\psi}+28e^{2i(\theta+\psi)}-28e^{6i(\theta+\psi)}+e^{8i(\theta+\psi)}+70e^{2i(2\theta+\psi)}$$
$$+28e^{2i(3\theta+\psi)}+e^{2i(4\theta+\psi)}-8e^{i(\theta+2\psi)}-56e^{3i(\theta+2\psi)}-10e^{4i(\theta+2\psi)}-28e^{2i(\theta+3\psi)}+4e^{2i(\theta+4\psi)}$$
$$-8e^{i(\theta+6\psi)}+4e^{i(\theta+8\psi)}]. \tag{C13}$$

$$Z_1 = \tfrac{1}{128}d_{11}e^{-i(4\theta+3\psi)}(e^{2i\theta}-1)^3[1+2e^{i\theta}+e^{2i\theta}+e^{6i\psi}+e^{2i(\theta+3\psi)}-2e^{i(\theta+6\psi)}], \tag{C14}$$

$$Z_2 = \tfrac{1}{128}d_{11}e^{-i(4\theta+3\psi)}(e^{2i\theta}-1)^3[1-2e^{i\theta}+e^{2i\theta}+e^{6i\psi}+e^{2i(\theta+3\psi)}+2e^{i(\theta+6\psi)}], \tag{C15}$$

$$Z_3 = -\tfrac{1}{256}d_{11}e^{-i(4\theta+3\psi)}(e^{2i\theta}-1)^3[1+2e^{i\theta}+e^{2i\theta}+e^{6i\psi}+e^{2i(\theta+3\psi)}-2e^{i(\theta+6\psi)}], \tag{C16}$$

$$Z_4 = -\tfrac{1}{256}d_{11}e^{-i(4\theta+3\psi)}(e^{2i\theta}-1)^3[1-2e^{i\theta}+e^{2i\theta}+e^{6i\psi}+e^{2i(\theta+3\psi)}+2e^{i(\theta+6\psi)}], \tag{C17}$$

$$Z_5 = -\tfrac{1}{256}d_{11}e^{-i(4\theta+3\psi)}(e^{2i\theta}-1)[1+6e^{i\theta}+15e^{2i\theta}+20e^{3i\theta}+15e^{4i\theta}+6e^{5i\theta}+e^{6i\theta}+15e^{4i\theta+6i\psi}-6e^{5i\theta+6i\psi}$$
$$+e^{6i\psi}+e^{6i(\theta+\psi)}-20e^{3i(\theta+2\psi)}+15e^{2i(\theta+3\psi)}-6e^{i(\theta+6\psi)}], \tag{C18}$$

$$Z_6 = -\tfrac{1}{256}d_{11}e^{-i(4\theta+3\psi)}(e^{2i\theta}-1)[1-6e^{i\theta}+15e^{2i\theta}-20e^{3i\theta}+15e^{4i\theta}-6e^{5i\theta}+e^{6i\theta}+15e^{4i\theta+6i\psi}+6e^{5i\theta+6i\psi}+e^{6i\psi}$$
$$+e^{6i(\theta+\psi)}+20e^{3i(\theta+2\psi)}+15e^{2i(\theta+3\psi)}+6e^{i(\theta+6\psi)}]. \tag{C19}$$

---

[1] P. A. Franken, G. Weinreich, C. W. Peters, and A. E. Hill, Generation of Optical Harmonics, Phys. Rev. Lett. **7**, 118 (1961).

[2] M. Bass, J. F. Ward, G. Weinreich, and P. A. Franken, Optical Rectification, Phys. Rev. Lett. **9**, 446 (1962).

[3] J. A. Giordmaine and R. C. Miller, Tunable Coherent Parametric Oscillation in LiNbO₃ at Optical Frequencies, Phys. Rev. Lett. **14**, 973 (1965).

[4] E. J. Woodbury and W. K. Ng, Ruby laser operation in near IR, Proc. IRE **50**, 2367 (1962).

[5] D. M. Lukin, C. Dory, M. A. Guidry, K. Y. Yang, S. D. Mishra, R. Trivedi, M. Radulaski, S. Sun, D. Vercruysse, G. H. Ahn, and J. Vuckovic, ⁴H-silicon-carbide-on-insulator for integrated quantum and nonlinear photonics, Nat. Photonics **14**, 330 (2020).

[6] C. Trovatello, A. Marini, X. Y. Xu, C. Lee, F. Liu, N. Curreli, C. Manzoni, S. Dal Conte, K. Yao, A. Ciattoni, J. Hone, X. Y. Zhu, P. J. Schuck, and G. Cerullo, Optical parametric amplification by monolayer transition metal dichalcogenides, Nat. Photonics **15**, 6 (2021).

[7] J. A. Armstrong, N. Bloembergen, J. Ducuing, and P. S. Pershan, Interactions between light waves in a nonlinear dielectric, Phys. Rev. **127**, 1918 (1962).

[8] Y. C. Wang, H. J. Zhang, H. H. Yu, Z. P. Wang, and J. Y. Wang, Light propagation in an optically active plate with topological charge, Appl. Phys. Lett. **101**, 171114 (2012).

[9] H. Rabin and P. P. Bey, Phase matching in harmonic generation employing optical rotatory dispersion, Phys. Rev. **156**, 1010 (1967).

[10] S. C. Chen and I. C. Khoo, Phase matching of second harmonic generations in rotational crystals, Appl. Opt. **26**, 186 (1987).

[11] S. Pancharatnam, Generalized theory of interference and its applications, Proc. Ind. Acad. Sci. **44**, 247 (1956).

[12] A. Tomita and R. Y. Chiao, Observation of Berry's Topological Phase by Use of an Optical Fiber, Phys. Rev. Lett. **57**, 937 (1986).

[13] M. V. Berry, The adiabatic phase and Pancharatnam's phase for polarized light, J. Mod. Opt. **34**, 1401 (1987).

[14] G. Milione, S. Evans, D. A. Nolan, and R. R. Alfano, Higher order Pancharatnam-Berry Phase and the Angular Momentum of Light, Phys. Rev. Lett. **108**, 190401 (2012).

[15] P. X. Ye, *Nonlinear Optical Physics* (Peking University Press, Peking, 2007).

[16] C. Li, *Nonlinear Optics: Principles and Applications* (Shanghai Jiao Tong University Press, Shanghai, 2017).

[17] R. J. Lingard and A. R. Renshaw, Determining the sign of optical rotation in linearly birefringent crystal sections, J. Appl. Crystallogr. **27**, 647 (1994).

[18] R. W. Boyd, *Nonlinear Optics* (Academic Press, Orlando, 2008).

[19] H. Poincare, *Theorie Mathematique de la Lumiere* (Gauthiers-Villars, Paris, 1892), Vol. 2.

[20] K. Charles, *Introduction to Solid State Physics* (Wiley, New York, 1996).

[21] Y. Chen, R. Ni, Y. D. Wu, L. Du, X. P. Hu, D. Z. Wei, Y. Zhang, and S. N. Zhu, Phase-matching Controlled Orbital Angular Momentum Conversion in Periodically Poled Crystals, Phys. Rev. Lett. **125**, 143901 (2020).

[22] T. Körner, A. Heinrich, M. Weckerle, P. Roocks, and B. Stritzker, Integration of magneto-optical active bismuth iron garnet on nongarnet substrates, J. Appl. Phys. **103**, 07B337 (2008).

[23] G. D. Miller, R. G. Batchko, W. M. Tulloch, D. R. Weise, M. M. Fejer, and R. L. Byer, 42%-efficient single-pass cw second-harmonic generation in periodically poled lithium niobate, Opt. Lett. **22**, 1834 (1997).

[24] L. Bi, J. Hu, P. Jiang, D. H. Kim, G. F. Dionne, L. C. Kimerling, and C. A. Ross, On-chip optical isolation in monolithically integrated non-reciprocal optical resonators, Nat. Photonics **5**, 758 (2011).

[25] K. Shui, L. Nie, Y. Zhang, B. Peng, J. Xie, L. Deng, and L. Bi, Design of a compact waveguide optical isolator based on multimode interferometers using magneto-optical oxide thin films grown on silicon-on-insulator substrates, Opt. Express **24**, 12856 (2016).

[26] G. Ryu, C. S. Yoon, T. P. J. Han, and H. G. Gallagher, Growth and characterisation of $CsLiB_6O_{10}$ (CLBO) crystals, J. Cryst. Growth **191**, 492 (1998).

[27] J. Herreros-Cedres, C. Hernandez-Rodriguez, and W. Kaminsky, Absolute optical rotation of $CsLiB_6O_{10}$, J. Appl. Crystallogr. **38**, 544 (2005).

[28] Y. Shopa, L. Lutsiv-Shumskiy, and R. Serkiz, Optical activity of the KDP group crystals, Ferroelectrics **317**, 271 (2005).

[29] S. J. Zhu, S. L. Wang, L. Liu, D. L. Wang, W. D. Li, P. P. Huang, and X. G. Xu, Refractive index homogeneity of large scale potassium dihydrogen phosphate crystal, Acta Phys. Sin. **63**, 107701 (2014).

[30] K. Kato and E. Takaoka, Sellmeier and thermo-optic dispersion formulas for KTP, Appl. Opt. **41**, 5040 (2002).

[31] C. Hernandez-Rodriguez, A. B. Fragoso-Lopez, J. Herreros-Cedres, and R. Guerrero-Lemus, Temperature-dependent optical rotatory power in the presence of birefringence of KTA and KTP crystals by the high-accuracy universal polarimeter method at 632.8 nm wavelength, J. Appl. Crystallogr. **47**, 566 (2014).

[32] J. Bohm, R. B. Heimann, M. Hengst, R. Roewer, and J. Schindler, Czochralski growth and characterization of piezoelectric single crystals with langasite structure: $La_3Ga_5SiO_{14}$ (LGS), $La_3Ga_{5.5}Nb_{0.5}O_{14}$ (LGN), and $La_3Ga_{5.5}Ta_{0.5}O_{14}$ (LGT): Part I, J. Cryst. Growth **204**, 128 (1999).

[33] F. Guo, D. Z. Lu, P. Segonds, J. Debray, H. H. Yu, H. J. Zhang, J. Y. Wang, and B. Boulanger, Phase-matching properties and refined Sellmeier equations of $La_3Ga_{5.5}Nb_{0.5}O_{14}$, Opt. Mater. Express **8**, 858 (2018).

[34] J. Etxebarria, C. L. Folcia, and J. Ortega, Origin of the optical activity of silver thiogallate, J. Appl. Crystallogr. **33**, 126 (2000).

[35] K. Kato, T. Okamoto, S. Grechin, and N. Umemura, New Sellmeier and thermo-optic dispersion formulas for $AgGaS_2$, Crystals **9**, 129 (2019).

[36] S. Marcinkevicius, G. Babonas, B. V. Korzun, and I. G. Tregub, Optical activity of semiconductors with chalcopyrite structure, Phys. Status Solidi B **135**, 615 (1986).

[37] J. Wei, J. M. Murray, F. K. Hopkins, D. M. Krein, K. T. Zawilski, P. G. Schunemann, and S. Guha, Measurement of refractive indices of $CdSiP_2$ at temperatures from 90 to 450 K, Opt. Mater. Express **8**, 235 (2018).

[38] D. E. Zelmon, E. A. Hanning, and P. G. Schunemann, Refractive-index measurements and Sellmeier coefficients for zinc germanium phosphide from 2 to 9 μm with implications for phase matching in optical frequency-conversion devices, J. Opt. Soc. Am. B **18**, 1307 (2001).

[39] M. Simon, F. Mersch, C. Kuper, S. Mendricks, S. Wevering, J. Imbrock, and E. Kratzig, Refractive indices of photorefractive bismuth titanate, barium-calcium titanate, bismuth germanium oxide, and lead germanate, Phys. Status Solidi A **159**, 559 (1997).

[40] N. C. Deliolanis, E. D. Vanidhis, and N. A. Vainos, Dispersion of electrogyration in sillenite crystals, Appl. Phys. B **85**, 591 (2006).